

Monte-Carlo simulations of the background of the coded-mask camera for X- and Gamma-rays on-board the Chinese-French GRB mission SVOM

O. Godet ^{a,*}, P. Sizun ^b, D. Barret ^c, P. Mandrou ^c
B. Cordier ^d, S. Schanne ^d & N. Remoué ^c

^a*X-ray and Observational Astronomy Group, Department of Physics &
Astronomy, University of Leicester, LE1 7RH, UK*

^b*CEA, IRFU, SEDI, 91191 Gif-sur-Yvette, France*

^c*Centre d'Etude Spatiale des Rayonnements, 9 avenue du Colonel Roche, 31047
Toulouse, France*

^d*CEA, IRFU, Service d'Astrophysique, 91191 Gif-sur-Yvette, France*

Abstract

For several decades now, wide-field coded mask cameras have been used with success to localise Gamma-ray bursts (GRBs). In these instruments, the event count rate is dominated by the photon background due to their large field of view and large effective area. It is therefore essential to estimate the instrument background expected in orbit during the early phases of the instrument design in order to optimise the scientific performances of the mission. We present here a detailed study of the instrument background and sensitivity of the coded-mask camera for X- and Gamma-rays (CXG) to be used in the detection and localisation of high-redshift GRBs on-board the international GRB mission SVOM. To compute the background spectrum, a Monte-Carlo approach was used to simulate the primary and secondary interactions between particles from the main components of the space environment that SVOM will encounter along its Low Earth Orbit (LEO) (with an altitude of 600 km and an inclination of $\sim 30^\circ$) and the body of the CXG. We consider the detailed mass model of the CXG in its latest design. According to our results, i) the design of the passive shield of the camera ensures that in the 4-50 keV imaging band the cosmic X-/Gamma-ray background is dominant whilst the internal background should start to become dominant above 70-90 keV; ii) the current camera design ensures that the CXG camera will be more sensitive to high-redshift GRBs than the *Swift* Burst Alert Telescope thanks to a low-energy threshold of 4 keV.

Key words: Monte-carlo simulation, background, Hard X-rays
PACS:

1 Introduction

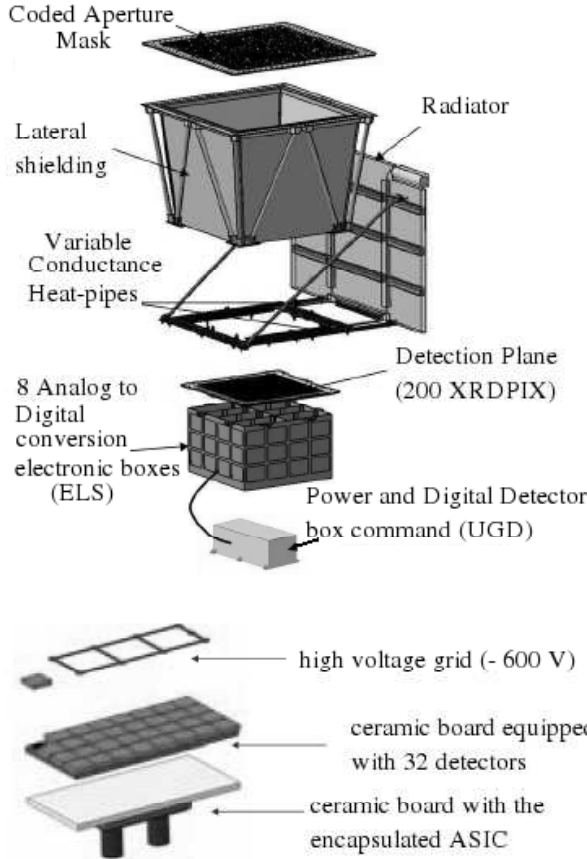
Gamma-ray bursts (GRBs) are highly transient and powerful cosmological events appearing in the sky for very short times (from a few milli-seconds to hundreds of seconds). They are considered to be associated to the death of massive stars [1] or compact object mergers [2]. Past and current space missions dedicated to the study of GRBs have demonstrated that the most efficient way to detect and localise them in the hard X-ray and Gamma-ray domain is to use wide-field coded-mask cameras.

We present here the main instrument of the science payload on-board the international GRB mission SVOM (Space Variable Object Monitor) [3,4], the coded-mask camera for X- and Gamma-rays (CXG) responsible for triggering GRB observations in the 4-250 keV energy band and their localisation with an accuracy better than 10 arc-minutes in the 4-50 keV imaging band. SVOM, which is the evolution of the mission *ECLAIRs* [5,6] from micro- to mini-satellite, is dedicated to the study of high-redshift GRBs. It is expected to be launched in 2013. The CXG has a large field of view (FoV ~ 2 sr). The CXG passive shielding is designed so that the background photons coming from outside the FoV will be completely absorbed by the compounds of the shielding (see Section 2.3 and Fig. 1). The detection plane, DPIX [7] with an effective area of 1024 cm² is an assembly of 200 elementary modules (XRDPIX) equipped with 32 CdTe Schottky detectors (4×4 mm², 1 mm thickness) produced by ACRO RAD Co. LTD in Japan (e.g. [8]). Each XRDPIX is read out by the very low noise front-end ASIC IDeF-X [9], which will enable the camera to reach a low-energy threshold of ~ 4 keV after careful selection of the 6400 CdTe detectors of the detection plane (see Fig. 1). First lab measurements using a CdTe detector coupled with IDeF-X reported a low-energy threshold around 2.7 keV (see Fig. 4 in [7]; see also [10]). This is a significant technological improvement when compared to the 12-15 keV low-energy threshold of the *Swift* BAT (Burst Alert Telescope) or INTEGRAL/ISGRI (Integral Soft Gamma-Ray Imager) using similar detectors. The CXG is currently in a B phase at the CNES (Centre National d'Etudes Spatiales, the French Space Agency).

* Corresponding author.

Email address: og19@star.le.ac.uk (O. Godet).

¹ Present address: CESR - 9 avenue du Colonel Roche, 31028 Toulouse Cedex 4, France. Tel: +33 561558371; Fax: +33 561556701



The XRDPIX elementary detection module

Energy range	Imaging : 4 keV to ~70 keV Detection : 4 keV to 250 keV
Field of view	~2 steradians
Angular resolution	~10 arcmin error radius (90% c.l.) for faintest sources, and ~2 arcmin for brightest ones
Photon timing	10 μ s
GRB duration detection range	from 10 ms to 1000 s
Coded aperture mask	Ta-W alloy (0.6 mm thick) 100x100 pixels (5.4 mm) 30% transparency Mask/detector distance = 46 cm
Lateral shielding	Pb (0.9 mm thick), Cu (0.1 mm), Al (0.5 mm) (to block X-ray diffuse background)
Detection plane	CdTe detectors (Schottky type : In/CdTe/Pt, from ACRO RAD Japan) ; $4 \times 4 \times 1 \text{ mm}^3$ Sensitive area = 1024 cm ² (80x80 detectors) Detector module : XRDPIX (32 detectors + 1 ASIC) Passive cooling : -20°C (modules fixed on cold plate) Spectral resolution < 2 keV

Fig. 1. View of ECLAIRs main components and summary of ECLAIRs main characteristics.

Coded-mask cameras such as the CXG are known to be photon background-dominated instruments due to their large FoV and effective area. Even if GRBs have high signal-to-noise ratios, it is still of primary importance to evaluate the camera background expected in orbit during the early phases of the design in order to optimise the instrument capability to observe GRBs as well as non GRB targets. This paper focuses on the estimation of the background spectrum of the CXG camera, depending on its design and mission parameters, and the impact on the scientific performances of the mission. This paper is organised as follows:

- §2 We give a brief description of the Monte-Carlo simulator, Geant, as well as the main components of the space environment that the spacecraft will encounter once in orbit, used to perform our simulations. We also define the mass model of the CXG camera used to perform our simulations.
- §3 We discuss the main features of the background spectrum. We also compute the camera limiting sensitivity for GRBs, and we compare it with those obtained with other GRB trigger instruments. We investigate what impact

on the camera performance would have the existence of a dead layer on the detectors.

§4 We present the main conclusions of the paper and discuss further improvements.

2 Monte-Carlo simulations of the instrument background

2.1 *Simulation tool*

The simulations were performed using the CERN Monte-Carlo code Geant², initially designed to model the interactions between matter and particles in high-energy nuclear physics experiments. Geant has since been used in the astrophysical field to model the performance of space instruments such as SPI (SPectrometer on INTEGRAL) on-board INTEGRAL [11] and Fermi/GLAST [12], for instance.

Geant enables us to: i) describe the detailed mass model of the payload and the spacecraft; ii) draw particles (photons, electrons, protons, neutrons, ...) following a specific spatial and energy distribution; iii) track the paths of the primary particles through the body of the camera and the spacecraft as well as any secondary particles generated during the different physical processes such as Compton, Rayleigh scattering, photo-electric effects, pair annihilation and creation, nuclear interaction.

The simulations were performed using the release 4.9.1 of the Geant4 C++ toolkit [13] along with the low energy electromagnetic physics dataset.

2.2 *Space environment and GRB model*

SVOM is a LEO mission with an altitude of 600 km and an inclination of 30° [3,4]. The satellite will then be subject to different sources of background in space: extragalactic components (X-ray and Gamma-ray diffuse background, primary proton and electron cosmic rays) and near Earth components (Gamma-ray albedo, neutrons, secondary protons located under the radiation belt). At the moment, we only take into account the extragalactic diffuse background, because it is the most relevant source of background for the study presented here (see Section 3.1).

² <http://geant4.web.cern.ch/geant4>

The main source of background radiation for a wide-field camera is the quasi-isotropic cosmic X-/Gamma-ray background [14]. The spectrum of the cosmic background that we used is from [15] (from 10 keV to 2 MeV). [16] showed that the *Swift*-BAT agrees within 8% with the normalisation of the cosmic background spectrum given in [15] below 2 MeV.

The cosmic background spectrum measured by *XMM-Newton* [17], RXTE [18] and *Chandra* [19] seems to be larger by 25-40% in the 2-10 keV energy range when compared to the spectrum given in [15]. [20] argued that the discrepancies between the different instruments in this energy band may be related to systematic errors in the response function used for diffuse sources. However, this discrepancy needs to be confirmed (see [21]).

For our simulations, we decided to extend the shape of the cosmic background spectrum given in [15] below 10 keV. We considered a 2π sr spatial distribution for the cosmic background photons in our simulations since the Earth acts like a screen on the other hemisphere.

2.2.1 GRB model

GRBs are assumed to be point-like sources with a spectral distribution given by the Band's function [22] as follows:

$$N(E) = A_0 \begin{cases} \left(\frac{E}{100 \text{ keV}}\right)^\alpha \exp\left(-\frac{E}{E_0}\right), & E \leq E_p \\ \left(\frac{E_0}{100 \text{ keV}}\right)^{(\alpha-\beta)} e^{(\beta-\alpha)} \left(\frac{E}{100 \text{ keV}}\right)^\beta, & E > E_p \end{cases}$$

where A_0 is in units of photons $\text{cm}^{-2} \text{s}^{-1} \text{keV}^{-1}$ and the peak energy $E_p = (\alpha - \beta) E_0$ is the energy for which the radiated energy reaches a maximum.

2.3 Mass model of the CXG camera

Below we describe the specifications of the mass model of the CXG camera used to perform the simulations following the mass and dimension restrictions of the SVOM mission. Table 1 summarises the main characteristics of the camera.

On-board the SVOM mission (see Fig. 2), the detection plane consists of 80×80 1 mm-thick CdTe pixels with a useful width of 4 mm, leading to an effective area of 1024 cm^2 . The ceramics supporting the detector and the ASIC are taken into account in the simulations. However, the high voltage grid is not modelled. Made of a Ta-W alloy, the 500 μm thick and 54 cm wide coded

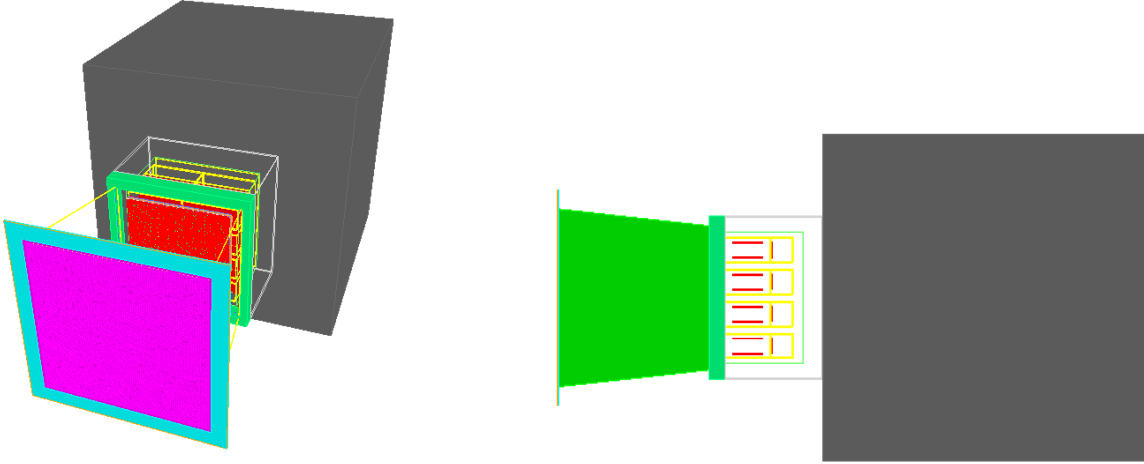


Fig. 2. Scheme of the mass model of the CXG as well as the cold plate and the readout electronics box placed under the camera, as designed for the mission SVOM (see Section 2.3). The grey box corresponds to the satellite platform.

mask, whose presently square pattern contains 30 percent open cells, is located about 46 cm above the detectors, which provides the instrument with a field of view of 2 sr. The mass model also includes a multi-layer thermal coating insulation (MLI) above the coded mask to prevent optical photon loading on the detection plane, the TA6V upper- and lower supports of the mask, as well as simplified versions of the cold plate in AlBeMet and the readout electronics box.

After simulations, we chose a graded shield combining Pb, Cu and Al, which is a trade-off between a maximum reduction of the background in the 4-50 keV energy band, mass budget considerations and the necessity to keep a few instrumental gamma-ray lines at higher energies for calibration purposes, especially lead $K\alpha$ and $K\beta$ fluorescence lines.

The remainder of the satellite is assumed to be a 1 m³ 300 kg cube of pseudo-Aluminium, which has an averaged density defined as the ratio of the spacecraft mass over its volume, the exact structure of the spacecraft being not yet known with accuracy.

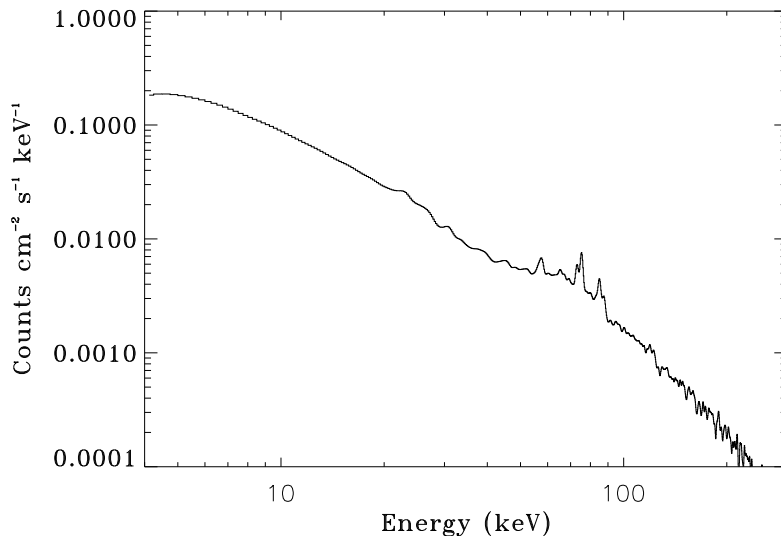


Fig. 3. Averaged spectrum of the background induced by the X-ray diffuse background (outside the South Atlantic Anomaly) on the detection plane of the CXG. The spectrum is degraded to the resolution of the CdTe detectors using a Gaussian with a FWHM of 1.6 keV as measured in the CCSR lab facility.

3 Results on the background level and the instrument sensitivity

3.1 The background spectrum

Fig. 3 shows the spectrum of the background measured on the detection plane resulting from our Monte-Carlo simulations in the 4 keV-300 keV energy range. The spectrum is degraded to the resolution of the CdTe detectors using a Gaussian with a FWHM of ~ 1.6 keV as measured in the CCSR lab facility.

The presence of the MLI layer on top of the coded mask results in a decrease of the background level at low energy, since it absorbs a fraction of the incident low-energy photons. Thus, the MLI layer is responsible for decreasing the background level by $\sim 11\%$, in the 4-50 keV energy band (see Fig. 9). The compounds and thicknesses of the passive shielding and the coded mask, as summarised in Table 1, lead to the apparition of several fluorescence lines (see Fig. 3 and Fig. 4; the line characteristics in Fig. 4 are from [23,24,25]). The intensity of the Au fluorescence lines coming from the electronics is likely to be overestimated due to the crude modelling of the electronics in our simulations at the moment. $K\alpha$ and $K\beta$ fluorescence lines from the Cd and Te are also seen in the background spectrum. The most intense instrumental lines (Pb-Ta lines) will be used to calibrate the gain of the detection plane in orbit. To ensure a better control on the gain over the energy band of the CXG camera (4-250 keV), we are investigating the benefit of considering some fluorescence

Element		Balmer						Lyman				
Z	Symb.	L α 2	L α 1	L β 1	L β 2	L γ 1	L γ 2	K α 2	K α 1	K β 3	K β 1	K β 2
48	Cd	3.13	3.13	3.32	3.53	3.72	3.95	22.98 (53.2)	23.17 (100)	26.06	26.10 (27.3)	26.6 (5.3)
50	Sn	3.44	3.44	3.66	3.90	4.13	4.38	25.04 (53.4)	25.27 (100)	28.44	28.49 (28.2)	29.1 (5.5)
52	Te	3.76	3.77	4.03	4.30	4.57	4.83	27.20 (53.7)	27.47 (100)	30.94	31.00 (28.8)	31.7 (5.8)
73	Ta	8.09	8.15	9.34	9.67	10.96	11.23	56.27 (57.4)	57.53 (100)	64.95	65.2 (33.7)	67.0 (8.5)
74	W	8.34	8.40	9.67	9.96	11.29	11.61	57.98 (57.6)	59.32 (100)	66.95	67.25 (33.8)	69.1 (8.6)
79	Au	9.63	9.71	11.44	11.58	13.38	13.71	66.99 (58.6)	68.80 (100)	77.58	77.98 (34.5)	80.2 (9.4)
82	Pb	10.45	10.55	12.61	12.62	14.76	15.10	72.81 (59.3)	74.97 (100)	84.45 (11.6)	84.94 (22.2)	87.3 (10.2)

Fig. 4. Summary of the fluorescence lines observed in the background spectra. The numbers mentioned in parenthesis correspond to the relative intensities of the lines [23]. The line energies come from [24]. Note that the values mentioned in the Table are slightly different from those used in Geant4 [25].

lines at low energy (for instance, Cu K α 8.04 keV) without degrading too much the scientific performances of the camera. From the simulations, we checked that the efficiency of the passive shielding to block the photon background outside the camera field of view is 100% in the 4-50 keV imaging band as required. The averaged background count rate in the 4-50 keV imaging band is 1.7 counts cm⁻² s⁻¹.

In addition to the external background (the X-ray diffuse background), the camera will present an internal background mainly due to charged particles interacting with the body of the camera. Even if we did not yet perform detailed simulations to model this background component, we can estimate that the CXG background should be dominated in the 4-50 keV imaging band (i.e. the relevant energy band here) by the X-ray diffuse background outside the SAA (South Atlantic Anomaly). Simulations outside the SAA on a previous design of the CXG camera to be embarked on-board the micro-satellite *ECLAIRs* showed that the transition between the internal (due to primary and secondary protons, primary electrons, neutrons and gamma-ray albedo) and external background (due to X-ray diffuse background) was expected to be around 100 keV [26]. Note that the two missions have similar orbital parameters (same altitude, but an inclination of 20° for *ECLAIRs* instead of 30° for SVOM) and the mass model of the *ECLAIRs*-CXG camera is fairly similar to that used on-board SVOM, and the compounds in both mass models have similar *Z*-values. The mass ratio of the CXG camera between SVOM and *ECLAIRs* is 4.2. We could then expect the internal background of the SVOM-CXG camera to be roughly four times larger than that computed for the *ECLAIRs*-CXG. This would result in a transition between the internal and external background to be around 70-90 keV.

3.2 Preliminary results on the instrument sensitivity

We used the formalism described in [27] to compute the 1-1000 keV limiting sensitivity of the camera (F) for different energy ranges of the CXG camera as a function of the GRB parameter, E_p . This enables us to compare directly the expected GRB sensitivity of the CXG with respect to other present and future GRB instruments [28] (see Fig. 5). To do so, we considered: i) GRB spectra with $\alpha = -0.5$ and $\beta = -2$ which are the averaged values derived from the BATSE α and β distributions; ii) GRBs located on the camera axis and an integration time of 1.0 s. We used a trigger threshold of 5.5σ .

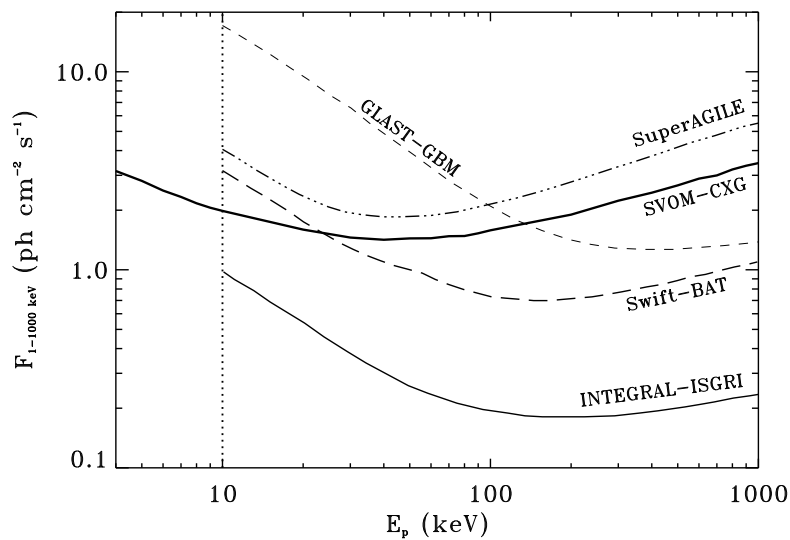


Fig. 5. Limiting sensitivity F in the $1 - 10^3$ keV energy range as a function of the GRB peak energy, E_p . The F -values of the CXG were computed using the 4-50 keV background level, an integration time of 1.0 s and a 5.5σ threshold as defined in [27]. We considered: i) GRB spectra with $\alpha = -0.5$ and $\beta = -2$; ii) GRBs located on the camera axis. The sensitivity values for other instruments come from [28] and were computed from $E_p = 10$ keV to $E_p = 1000$ keV.

From Fig. 5, it appears that the instrument ISGRI on-board INTEGRAL is the most sensitive instrument. However, its field of view is much smaller than that of the *Swift*-BAT, SuperAGILE, Fermi-GBM and SVOM-CXG. The CXG will be more sensitive to GRBs with $E_p < 20$ keV than most of the present and future high-energy instruments except ISGRI, and hence, to high-redshift GRBs of which the prompt radiation should peak mostly in X-rays. That is mainly due to the lower energy threshold of the CXG of ~ 4 keV (see Fig. 6) instead of 15 keV for the *Swift*-BAT for instance. However, the effective area of the CXG being less than that of the *Swift*-BAT (5200 cm²), the CXG will be less sensitive than the *Swift*-BAT to GRBs with $E_p > 20$ keV. Taking into account a broader energy range for the CXG background will only result in a

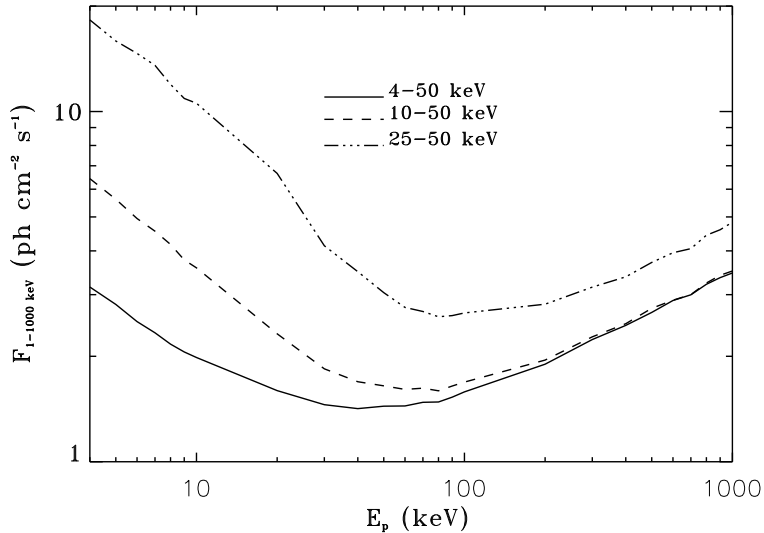


Fig. 6. Same as Fig. 5 for three different energy bands: 4-50 keV (solid line); 10-50 keV (dotted line); 25-50 keV (dashed line). As shown, the low energy threshold of the CXG at 4 keV is essential to enable the CXG to be more sensitive to high-redshift bursts than the *Swift*/BAT.

slight improvement of the CXG sensitivity at higher E_p -values. The CXG will also be more sensitive to GRBs with $E_p < 100$ keV than the GBM on-board Fermi/GLAST.

[29] reviewed the performance of current and future GRB missions to detect high-redshift GRBs. Their Table 1 shows that the current design of the SVOM-CXG may be enabled to detect 2-4 GRBs with a redshift larger than 6 per year.

3.3 Impact of a dead layer in the CdTe detectors on the CXG performance

Until then, we assumed all the CdTe detectors in the detection plane were described as pure CdTe crystals. We then did not model the Schottky contact on each detector (the anode) made of a ~ 300 nm thick Indium (In) layer + ~ 30 nm-thick Titanium (Ti) layer and the cathode made of a 200 – 300 nm Platinum (Pt) layer. The Ti layer is added to reinforce the stability of the In layer. Figure 7 shows a scheme of a CdTe detector. The incident photons will penetrate the detectors on the cathode. The Pt layer acts then like a dead layer on top the active volume of the detector. Even if this Pt layer is thin, it will absorb a significant fraction of low-energy photons, since the Pt layer results in an absorption of $\sim 40\%$ at 4 keV and $\sim 20\%$ at 6 keV (see Fig 8). Above 20 keV, the absorption is less than 5%. A full characterisation of the Pt dead layer thickness for each detector is under investigation at the CESR

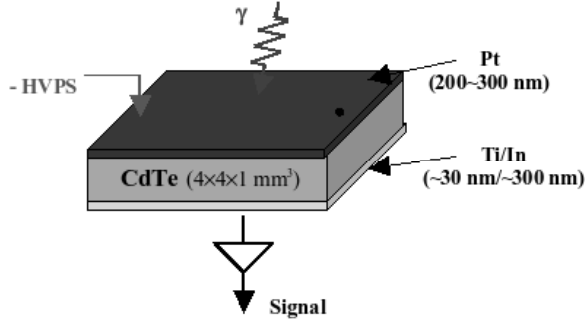


Fig. 7. Scheme of a Schottky CdTe detector provided by ACRO RAD Co. LTD. In addition of the CdTe active volume, the detector consists of a cathode made of a 200 – 300 nm Platinum (Pt) layer and an anode made of a ~ 300 nm thick Indium (In) + ~ 30 nm-thick Titanium (Ti) layer. The photons illuminating the cathode side of the detectors, the Pt layer acts like a dead layer absorbing low-energy photons.

lab facility [30]. In order to quantify the impact of such a dead layer on the CXG performance, we run Monte-Carlo simulations including a 250 nm-thick Pt dead layer on top each of pixels to model the cathode and a 300 nm thick Indium (In) layer + 30 nm-thick Titanium (Ti) layer to model the anode.

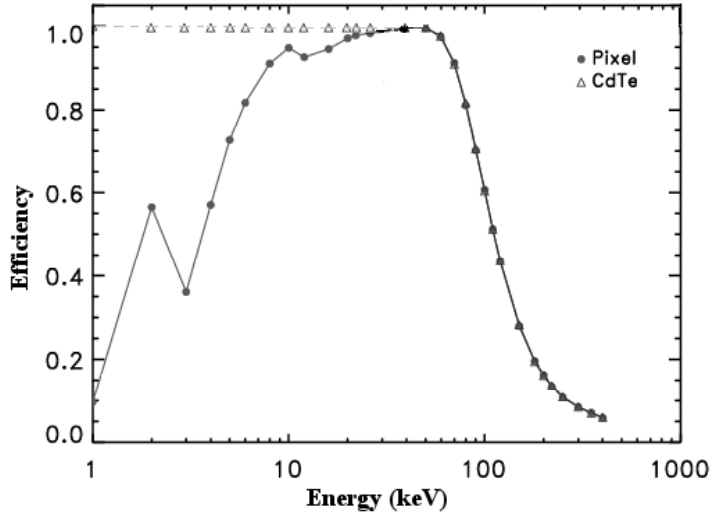


Fig. 8. Comparison of the efficiency of a CdTe pixel without (full triangles) and with (full circles) a 250 nm-thick Pt layer. The Pt layer results in an absorption of $\sim 40\%$ at 4 keV and $\sim 20\%$ at 6 keV. A full characterisation of the Pt dead layer thickness for each detector is under investigation at the CESR lab facility [30].

Fig. 9 shows the background spectrum of the CXG in the 4-50 keV energy band in three cases: without the MLI layer and the Pt dead layer (square – CASE₁); with the MLI layer, but without the Pt dead layer (crosses – CASE₂); with both (triangles – CASE₃). The effects of the MLI and dead layer are clearly visible at low energy. The introduction of the dead layer in our simulations results in a 40% decrease in the background level at 4 keV. The count rate

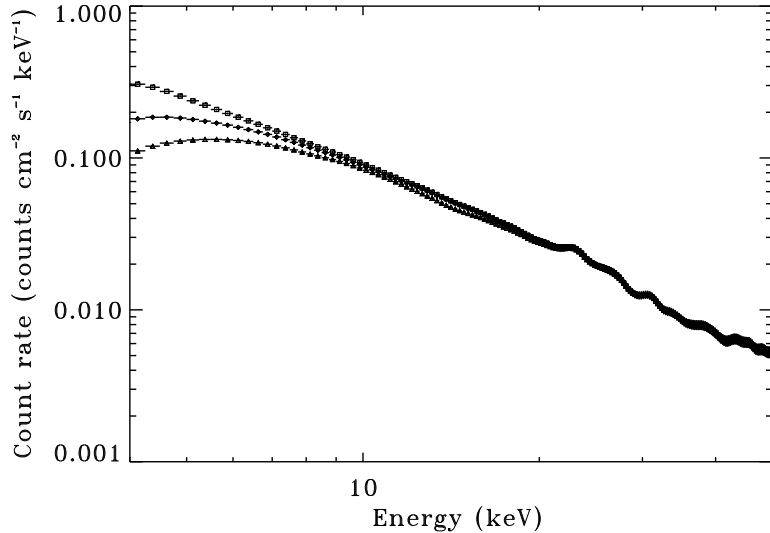


Fig. 9. Background spectrum in the 4-50 keV energy band illustrating the effects of the MLI and Pt layer: (squares) without the MLI and Pt layer; (crosses) with the MLI layer and without the Pt layer; (triangles) with both.

level is then $1.5 \text{ counts cm}^{-2} \text{ s}^{-1}$ in the 4-50 keV energy band (*i.e.* a 12% reduction with respect to the value found without the Pt cathode).

Fig. 10 shows the limiting sensitivity in the 1-1000 keV energy band as a function of the energy peak E_p in different cases. While the MLI induces a degradation of the sensitivity by less than 6% below $E_p = 10$ keV when compared to CASE_1 , the Pt cathode degrades the limiting sensitivity by less than 10% below $E_p = 10$ keV when compared to CASE_2 . The impact of the Pt dead layer on the CXG performance is not significant enough to change the main remarks drawn in Section 3.2.

4 Discussion and Conclusion

We described in detail our Monte-Carlo simulator to compute the background spectrum using a given mass model of the coded-mask camera CXG as well as a model of the spacecraft environment in orbit. We showed that the current design of the passive shield ensures that in the 4-50 keV imaging energy band, the background is dominated by the cosmic background. We showed that the MLI layer and the Pt cathode induce a significant reduction of the background count rate at low energy.

We demonstrated, using the estimated background level in the 4-50 keV imaging energy band, that the CXG will be more sensitive to GRBs with $E_p < 20$

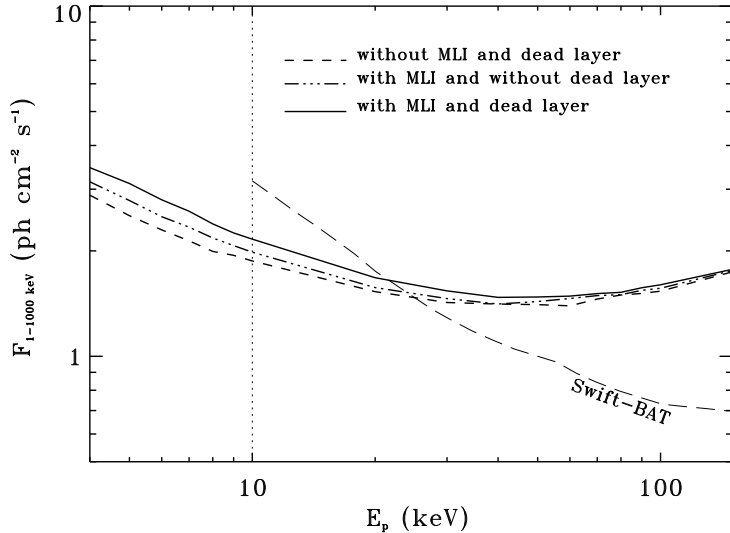


Fig. 10. Same as Fig. 5, but assuming 3 different cases: (dashed line) without the MLI layer and the Pt dead layer; (dashed and dotted line) with the MLI layer and without the Pt dead layer; (solid line) with both. Even when taking into account the Pt dead layer, the CXG should be more sensitive than the *Swift*-BAT to detect GRBs with $E_p < 20$ keV.

keV, thanks to an expected low-energy threshold around 4 keV, (and therefore potential high-redshift GRBs) than the *Swift*-BAT, presently the best-designed high-energy GRB imager to date. Computation showed that SVOM could detect a good sample of high-redshift GRBs during its lifetime.

We also showed that the MLI layer and the Pt cathode induce a non negligible decrease of the camera sensitivity for values of $E_p < 10$ keV. Investigation are on-going to see whether or not it is possible further to reduce the thickness of the MLI layer.

Further improvements will be also made in our simulator to refine results concerning: i) the internal background due the material activation in orbit; ii) the evolution of the background level near and in the SAA. We will also investigate the impact on the CXG performance of a higher contribution of the cosmic background below 10 keV.

We are also investigating the benefit to use a coded mask with an aperture of 40%, instead of 30% as presented in this paper, in order to increase the fraction of short GRBs detectable by the CXG without degrading too much the sensitivity of the camera.

The imaging performance of the CXG will be reviewed in a forthcoming paper.

Acknowledgements

OG gratefully acknowledges STFC funding and the CESR that hosted him during the writing of this paper, and where most of this work was done during his PhD.

References

- [1] MacFayden, A. I. & Woosley, S. E., *ApJ*, **524**, 262 (1999)
- [2] Eichler, D. et al., *Nature*, **340**, 126 (1989)
- [3] Schanne, S. et al., proceedings of the “30th International Cosmic Ray Conference (ICRC)”, 3-12 July, Merida, Yucatan, Mexico, arXiv:0711.3754 (2007)
- [4] Schanne, S., Proceedings of Gamma-Ray Bursts 2007 conference, Santa Fe, USA, 5-9 November 2007. Published in *AIP conf. proc.*, **1000**, 581 (2008)
- [5] Barret, D. et al., astro-ph/0205346 (2004)
- [6] Schanne, S. et al., *Nucl. Instr. and Meth. A*, **567**, 327 (2006)
- [7] Ehanno, M. et al., *Advances in Space Research*, **40**, 1259 (2007)
- [8] Takahashi, T. et al., *IEEE Trans. Nucl. Sci.*, **49**, 1297 (2002)
- [9] Gevin, O. et al., *IEEE NSS-MIC conference in Rome 2004* (2005)
- [10] Remoué, N. et al., *Proc. SPIE*, in press (2008)
- [11] Sturmer, S. J. et al., *A&A*, **411**, 81 (2003)
- [12] Kippen, R. M. et al., *THE FIRST GLAST SYMPOSIUM. AIP Conference Proceedings*, **921**, 590 (2007)
- [13] Agostinelli et al., *Nucl. Instr. and Meth. A*, **506**, 250 (2003)
- [14] Giacconi, R., Gursky, H., Paolini, F. R., Rossi, B. B., *Physical Review Letters*, **9**, 439 (1962)
- [15] Grüber, D. E., Matteson, J. L., Peterson, L. E., Jung, G. V., *ApJ*, **520**, 124 (1999)
- [16] Ajello, M. et al., *ApJ*, arXiv:0808.3377, in press (2008)
- [17] De Luca, A. & Molendi, S., *A&A*, **419**, 837 (2004)
- [18] Revnivtsev, M. et al., *A&A*, **444**, 381 (2005)
- [19] Hickox, R.C. & Markevitch, M., *ApJ*, **645**, 95 (2006)
- [20] Frontera, F. et al., *ApJ*, **666**, 86 (2007)

- [21] Moretti, A. et al., *A&A*, in press (2008)
- [22] Band, D. L., Matteson, J., Ford, L. et al., *ApJ*, **413**, 281 (1993)
- [23] Lederer, C. M. & Shirley, V. S., eds. *Table of Isotopes*, 7th ed. (1978)
- [24] Deslattes, R. et al., *National Institute of Standards and Technology* (2007)
- [25] Guatelli, S. et al., *IEEE Transactions on Nuclear Science*, **54**, 594 (2007)
- [26] Godet, O., Thesis, “Monte-Carlo simulations of the wide-field coded mask camera of the GRB mission *ECLAIRs*” (2005)
- [27] Band, D. L., *ApJ*, **588**, 945 (2003)
- [28] Band, D. L., arXiv:0801.4961 (2008)
- [29] Salvaterra, R., Campana, S., Chincarini, G., Tagliaferri, G., Covino, S., *MNRAS*, **380**, 45 (2007)
- [30] Remoué, N. et al. in preparation

Table 1

Summary of the main characteristics of the CXG camera as designed for the mission SVOM as well as the mission details.

Orbit:	Altitude = 600 km Inclination = 30°
Camera: Mass of the camera Mass of the platform Mask-detector plane height	~ 63 kg 300 kg 46 cm
Detection plane: Number of pixels Detector surface Detector thickness Efficient surface	80 × 80 4 × 4 mm ² 1 mm 1024 cm ²
Passive shielding: Compounds ⁺ Absorption in 4-50 keV*	Pb (0.9 mm), Cu (0.1 mm), Al (0.5 mm) 100%
Coded mask: Aperture fraction Compounds	30% TaW alloy (97.5% Ta & 2.5%W) [†] MLI layer [‡] 50 μm of Kapton, 12 μm of Mylar 0.5 μm of Al
Field of view: Total FoV totally coded FoV	88.7° × 88.7° (2.04 sr) 22.1° × 22.1° (0.15 sr)

⁺ The compounds are given from the outside to the inside.

^{*} The imaging energy band of the CXG camera.

[†] The percentages are given as a fraction of the 2.9 kg coded-mask mass.

[‡] The MLI layer will be put on top of the coded mask to prevent optical photon loading on the detection plane.